Int. J. Multiphase Flow Vol. 14, No. 3, pp. 349–359, 1988
Printed in Great Britain.

0301-9322/88 $3.00 + 0.00

HEAT TRANSFER IN THE PRESENCE OF CONDENSATE DRAINAGE

A. A. NICOL,[1] Z. L. AIDOUN,[2] R. J. GRIBBEN[3] and G. WILKS[4]

Departments of [1]Mechanical and Process Engineering and [3]Mathematics, University of Strathclyde, Glasgow, Scotland

[2]Department of Mechanical Engineering, Ecole Nationale Polytechnique, El-Harrach, Algeria

[4]Department of Mathematics, University of Keele, Keele, England

(*Received* 7 *May* 1987; *in revised form* 24 *December* 1987)

Abstract—Drainage mechanisms and the associated heat transfer coefficients have been investigated for steam condensing in the pressure range 0.2–0.66 b on three horizontal water-cooled tubes arranged in a vertical column. Controlled rates of inundation were obtained by recycling condensate through a row of small holes drilled in a fourth tube. The steam heat transfer coefficient showed a sharp reduction with increase in condensate film Reynolds number, becoming almost asymptotic at Re = 500.

Observations and measurements of the drainage re-attachment on lower tubes showed smooth assimilation of the columns into the liquid film with very little thickening of the film close to the points of impingement. Based on this evidence, a new theory for film drainage, describing film behaviour at the top of the tube more realistically than has been done previously has been developed and compared with experimental heat transfer coefficients Reynolds numbers up to 1000, which corresponds to the onset of film drainage.

Key Words: condensation, drainage, steam, tubes.

1. INTRODUCTION

One of the many problems in condenser design is that of estimating the effect of condensate drainage on the vapour side heat transfer coefficient. In the absence of drip trays inundation can be extremely heavy in the lower regions of large tube bundles as a result of the accumulation of condensate from the tubes above.

The first theoretical attempt to account for the influence of drainage was made by Nusselt (1916), whose analysis of a smooth laminar sheet of liquid flowing over a vertical column of tubes is known to underestimate the heat transfer coefficient as a result of differences between the assumed and actual drainage modes. Actual drainage has been observed to be rippled and discontinuous in contrast to the drainage film assumed by Nusselt. Furthermore, Nusselt's theory does not allow for radial flow velocities and so the prediction of the film thickness is incorrect at the top and bottom of the tubes. However, even though these deficiencies were recognized, Nusselt's theory was used as a reference for many years. Grant & Osment (1958) and Nobbs & Mayhew (1975) have both made experimental heat transfer studies using controlled inundation, while Berman & Tumanov (1962) and Fuks (1957) have reported work on tube bundles. Short & Brown (1951) and Kern (1958) both obtained relationships for the variation of the heat transfer coefficient with number of tube rows in a tube bundle, and Butterworth (1981) has compared and summarised the correlations quoted in these earlier papers. Shklover & Buevich (1978) and, more recently, Fujii & Oda (1983) have attempted to derive relationships between heat transfer coefficients and depth of tube bundle using models assuming more realistic modes of drainage.

The present work was undertaken to gain a better understanding of the detailed way in which the various modes of drainage, viz. drops, columns or sheets, influence condensation on a single tube. The results were to assist in the development of theoretical solutions to these localised drainage problems as well as to provide information for the development of a more comprehensive model for a tube bundle.

2. EXPERIMENTAL WORK

Figure 1 shows a line diagram of the general layout of the experimental apparatus. The low-pressure steam for use in the experimental condenser was generated in the boiler by passing

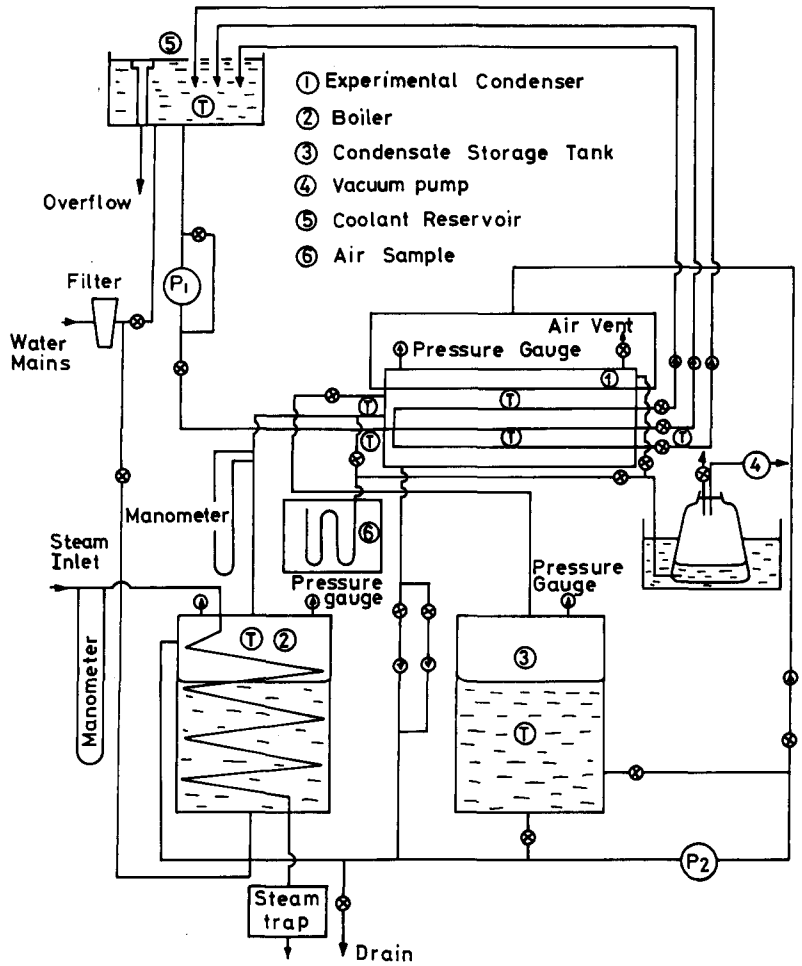

Figure 1. General layout of the condensation facility.

high-pressure steam through a copper coil immersed in the de-aerated feed water for the loop. The steam generated then flowed to the condenser and returned as condensate to the boiler via the storage tank. A second loop allowed condensate to be pumped from the storage tank to the perforated top tube. The cooling water was taken from the coolant reservoir, pumped through the three water-cooled tubes in the condenser and then returned to the reservoir. A vacuum pump, connected to the high point in the condenser cylinder, assisted in maintaining the operating pressure and was also used to extract the air in the loop during the de-aerating procedure prior to taking measurements.

The body of the experimental condenser was a glass cylinder 300 mm dia, 13 mm thick wall and 500 mm long, as shown in figure 2. The glass allowed visual and photographic observation of the modes of condensation. The end covers were machined from brass to give more freedom in accommodating the tubing and instrumentation within the condenser. Steam entered the condenser through one of the end covers and then passed through a short baffled region before encountering the condenser tubes.

The test section consisted of four copper tubes housed within the experimental condenser. Cooling water flowed through the three lower copper tubes, 19.06 mm o.d., 16.56 mm i.d., on which condensation took place. The working length of each tube was 300 mm with the remaining section of tube on either side insulated. The tubes were fed from a common header of 50 mm dia, in which provision was made for good mixing and even distribution of the cooling water among the tubes. Each tube had a control valve at the outlet for fine control of the flow rate. The top tube, or drainage tube, had a row of holes 0.5 mm dia, 1 mm pitch over its 300 mm working length. To isolate the tubes, thermally, from the brass end covers, all four tubes were secured to the end covers by polypropylene glands.

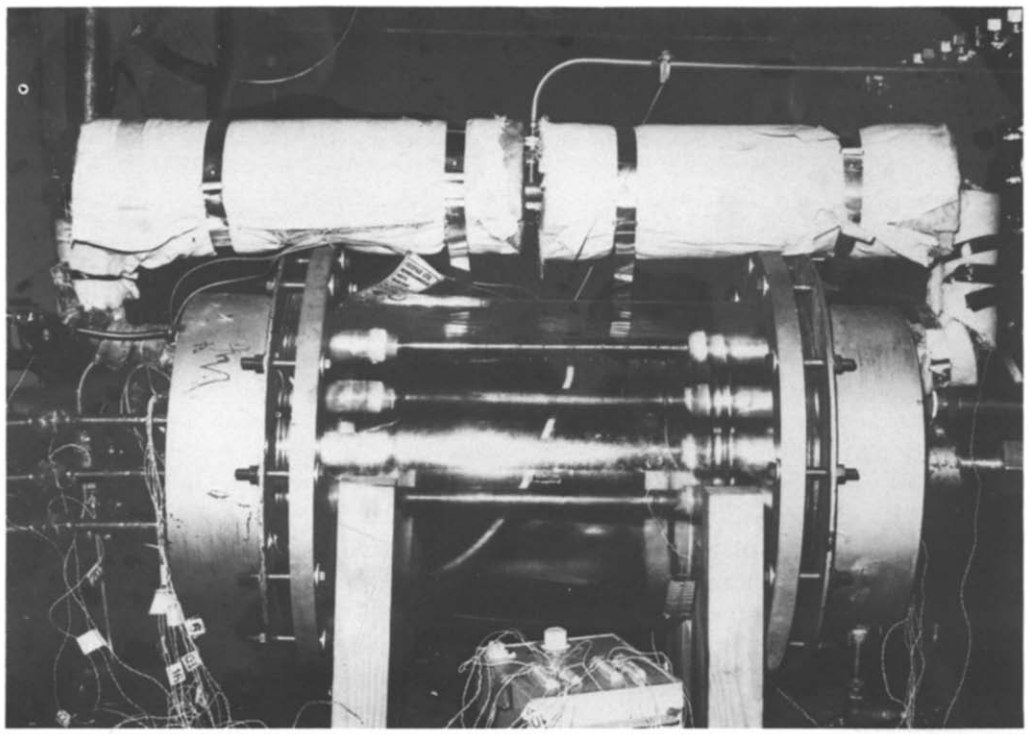

Figure 2. Experimental condenser.

Vapour and cooling water temperatures were determined using copper–constantan thermocouples located at appropriate points. The vapour or steam temperature was obtained from two thermocouples placed inside the condenser and during operation the steam condition was arranged to be slightly superheated at entry to the condenser. The cooling water entered the three tubes from a common, insulated header, into which two thermocouples were inserted to give the inlet cooling water temperature. Care was taken in the measurement of the average water temperature at outlet, as the cooling water temperature rise through each tube is important in calculating the heat transferred from the condensing steam. The smallest temperature rise was about 4°C which corresponded to the highest cooling water flow rate. Two thermocouples were placed at the outlet from each tube, after right-angled bends to encourage mixing, with another thermocouple located a few diameters downstream. In all cases the thermocouple wires were encased in a stainless-steel hypodermic sheath with only the bead projecting. This probe was then secured in position through a hole in the tube wall using a water-resistant resin.

All tests were made under conditions of low steam velocity and minimum air or non-condensable content in the vapour. The water in the condensing loop was de-gassed by allowing the loop to operate for a number of hours while removing separated air in the condenser using a vacuum pump connected to a tapping at the high point in the cylinder. Air leakage into the condenser and associated connecting pipework was reduced as far as possible by coating all joints with polyurethane varnish or Araldite resin and as a result the loop could maintain a high vacuum over a long period of time.

Tests were carried out for a range of pressures and both the overall and condensation heat transfer coefficients were determined from the measurements taken. The overall coefficient, U, was obtained by dividing the heat transferred to the cooling water by the logarithmic mean temperature difference, so taking account of the slight rise in cooling water temperature, and also by the outside area of the tube exposed to the steam. The steam heat transfer coefficient, h_s, was then calculated by subtraction of all the other resistances from the overall resistance, i.e. from

$$\frac{1}{h_s} = \frac{1}{U} - \frac{D_i}{D_o h_L} - R_w, \qquad [1]$$

where D_i and D_o are the inner and outer diameters of the tube and R_w is the wall thermal resistance.

The cooling water heat transfer coefficient, h_L was evaluated using the special Wilson plot method referred to by Mayhew (1981). The same form of correlating equation as used by Nobbs & Mayhew (1975) was chosen for the cooling water side heat transfer coefficient. Tests on the top tube for a range of pressures and cooling water flow rates gave heat transfer coefficients of 4–5% higher than the Nusselt values and in agreement with other workers.

3. CONDENSATION HEAT TRANSFER COEFFICIENTS

Figure 3 shows the variation of condensation heat transfer coefficient for the three tubes with Re_F for a cooling water Reynolds number, Re_{cw}, of 26,000 and vapour pressure 0.2 b. The difference in heat transfer coefficient, h_s, between the three tubes is most noticeable at zero drainage rate, i.e. where no artificial drainage from the top tube has been introduced. As Re_F increases, the effects of the additional drainage from tube to tube because of condensation is quickly suppressed by the influence of the much larger drainage flows such that the variation between the tubes is only just detectable over most of the range.

Figure 4 shows the dimensionless heat transfer coefficient h_s/h_1 for the top tube, for pressures of 0.2 and 0.66 b and a range of cooling water flow rates plotted against the ratio $(\Gamma + m)/m$, where h_s is the condensation heat transfer coefficient for different drainage rates, h_1 is the value of h_s for the 1st tube with zero inundation, i.e. the Nusselt value, Γ is the recirculated condensate flow rate and m is the additional condensate generated on the 1st tube. These results can also be interpreted as the variation in condensation heat transfer coefficient throughout a hypothetical tube bundle. The data are consistently above the equation recommended by Grant & Osment (1958) from their experiments on a tube bundle and above the equation of Short & Brown (1951). As these two equations were obtained from data on typical condenser tube bundles it is possible that the present data lie slightly above previous data due to the low air content in the experimental condenser. The controlled method of introducing the recirculated condensate compared to the "rain" from perhaps several higher tubes could also contribute to the difference. Agreement improves for values of $(\Gamma + m)/m > 50$.

4. MODES OF DRAINAGE

The glass-walled condenser allowed easy observation of the way in which condensate drained from tube to tube, as well as allowing comparisons to be made between the three condensing tubes.

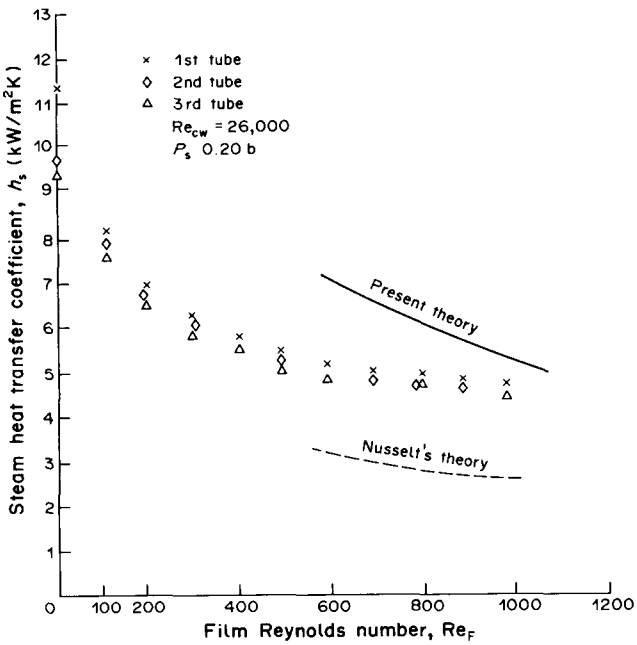

Figure 3. Effect of Re_f on h_s.

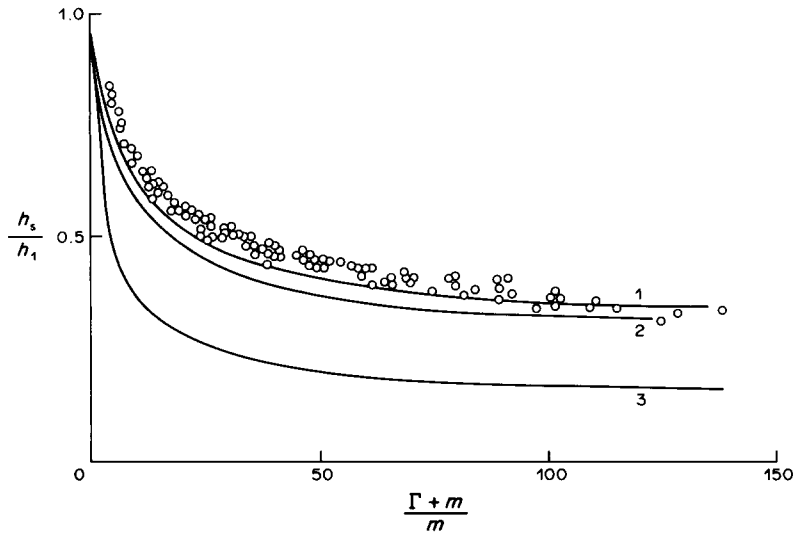

Figure 4. The dimensionless heat transfer coefficient as a function of dimensionless drainage: (1) Grant & Osment (1958), $h_s/h_l = [(\Gamma + m)/m]^{-0.223}$; (2) Short & Brown (1951), $h_s/h_l = [(\Gamma + m)/m]^{-0.25}$; (3) Nusselt (1916).

The modes of drainage reproduced those reported by Nicol & Aidoun (1984) for air–water simulation experiments and are shown in figure 5.

The condensate first of all separates from the tube in drops from selected sites for low Reynolds numbers but as the Reynolds number increases, column drainage is gradually established until all possible sites are active at a Reynolds number of 350. The film Reynolds number Re_F is defined as $2\Gamma/\mu$, where Γ is the mass flow of liquid or condensate flowing on to the tube per unit length and μ is the dynamic viscosity of the liquid film evaluated at the mean film temperature. At very high Reynolds numbers of about 800, partial film drainage is noticed between some adjacent sites but surface tension causes the film to break down into columns again before contact with the lower tube. The size and frequency of separation of drops and the spacing between columns is as reported by Nicol & Aidoun (1984). No splashing or loss of condensate between tubes was observed to take place even for the larger than typical condenser spacing between the tubes.

Observation of the re-attachement of the columns and film, and measurements of film thickness adjacent to the point of impingement, showed no evidence of thickening of the film at the top of the tube to the extent of that predicted by the Nusselt theory. Consequently, it was thought that an analysis treating the re-attachment problem as one of stagnation flow would more correctly model the liquid film behaviour at angular positions close to the top of the tube.

5. ASYMPTOTIC FILM DRAINAGE MODEL

The draining film of condensate is modelled as a two-dimensional jet of thickness $2h_0$ falling under gravity on to the upper region of the cylinder below with velocity U_0. The condensate

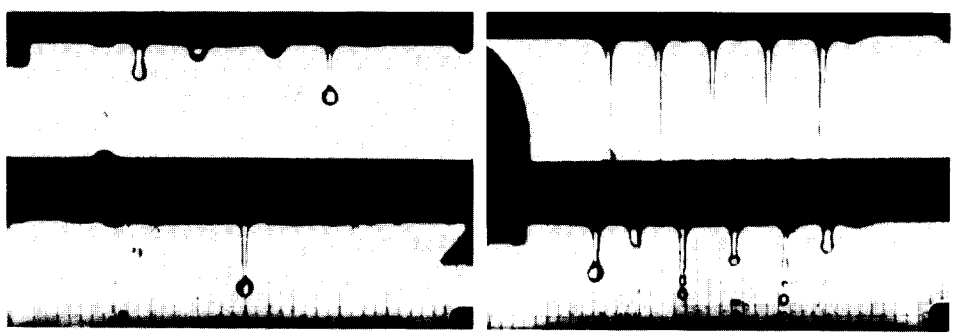

Figure 5. Drainage regimes—drops and columns.

impinges on the lower cylinder, radius a_0, as a spreading jet which develops into a smooth laminar film flow. At high drainage rates the additional mass of condensate due to condensation on to the cylinder is small and is therefore neglected.

The governing equations are taken as the Navier–Stokes equations and the equation of conservation of energy in plane polar coordinates (r, ϕ) with associated velocity components (v_r, v_ϕ), respectively. On the assumption that the semi-film thickness h_0 is small compared to the radius a_0, the following non-dimensional variables are introduced:

$$y = \frac{r - a_0}{h_0}, \quad x = \frac{\bar{x}}{a_0} = \phi, \quad v = \frac{a_0 v_r}{h_0 U_0}, \quad u = \frac{v_\phi}{U_0}$$

and

$$\theta = \frac{T - T_s}{T_w - T_s},$$

where $\bar{x}$ is the distance measured around the cylinder from the upper generator. In the absence of an imposed pressure gradient around the cylinder the reduced equations now read, after neglecting terms of $O(v/U_0 h_0, h_0/a_0)$,

$$\frac{\partial u}{\partial x} + \frac{\partial v}{\partial y} = 0, \tag{2}$$

$$u\frac{\partial u}{\partial x} + v\frac{\partial u}{\partial y} = \frac{\sin x}{\mathrm{Fr}} + \frac{\beta}{\mathrm{Fr}}\frac{\partial^2 u}{\partial y^2}, \tag{3}$$

$$\frac{\partial p}{\partial y} = 0 \tag{4}$$

and

$$u\frac{\partial \theta}{\partial x} + v\frac{\partial \theta}{\partial y} = \frac{\beta}{\mathrm{FrPr}}\frac{\partial^2 \theta}{\partial y^2}, \tag{5}$$

where

$\mathrm{Fr} = \dfrac{U_0^2}{g a_0}$ is the Froude number,

$\beta = \dfrac{\nu U_0}{g h_0^2}$

and

$\mathrm{Pr} = \dfrac{c_p \mu}{k}$ is the Prandtl number.

Notice that β may be written as $(a_0^2/h_0^2)/(1/\mathrm{Re}_{a_0})$, where $\mathrm{Re}_{a_0} = U_0 a_0/\nu$ is a Reynolds number based on the radius of the cylinder. Consequently, the last terms in [3] and [5] should be retained despite $\mathrm{Re}_{a_0} \gg 1$, so long as $h_0/a_0 \sim \mathrm{Re}_{a_0}^{-0.5}$.

The flow field boundary conditions are

$$u = v = 0 \quad \text{on} \quad y = 0 \qquad \frac{\partial u}{\partial y} = 0 \quad \text{on} \quad y = \delta(x), \tag{6}$$

where $\delta(x)$ is the dimensionless thickness of the liquid film. Subsequent to impingement, the conservation of volumetric flow rate, q, per unit length of cylinder requires that the flow field must further satisfy the constraint

$$\frac{q}{h_0 u_0} = \int_0^{\delta(x)} u \, dy = 1. \tag{7}$$

The simplest boundary conditions on temperature are adopted,

$$\theta = 1 \quad \text{on} \quad y = 0 \qquad [8]$$

and

$$\theta = 0 \quad \text{on} \quad y = \delta(x). \qquad [9]$$

These conditions correspond to a constant temperature T_w at the surface of the cylinder and to a constant temperature of the ambient steam T_s at the surface of the liquid film.

6. FLOW STRUCTURE

At the upper generator of the cylinder a viscous stagnation point flow will be embedded within the deflected inviscid semi-jet. Accordingly, the anticipated structure is illustrated in figure 6 where the designated Region I relates to that regime of flow between the top of the cylinder and the point at which viscous effects eventually are significant throughout the entire film. Figure 6 further illustrates the implications for the temperature field for condensate whose $\mathrm{Pr} > 1$. At the stage where viscous effects penetrate the film surface the thermal boundary layer thickness remains less than the local film thickness. As a result, Region II is anticipated in which the thermal boundary layer continues to grow whilst the velocity field adjusts towards a film flow dominated by a balance

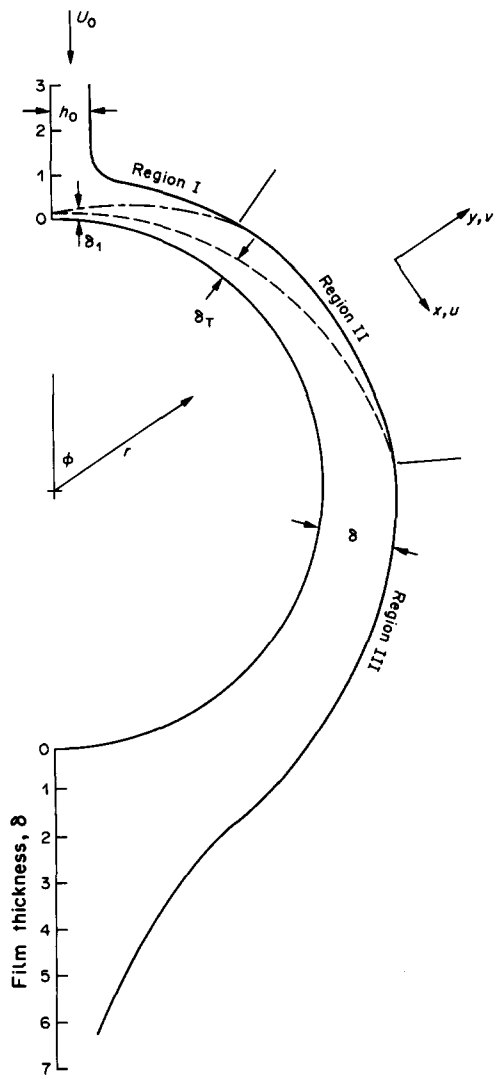

Figure 6. Film structure around the cylinder.

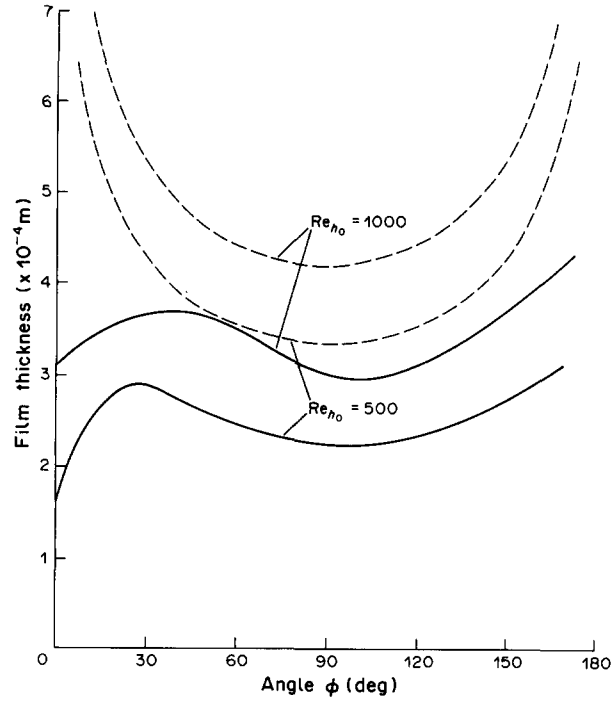

Figure 7.Film thickness comparison: ---- Nusselt (1916); —— theory.

of gravitational and viscous forces. Ultimately, in Region III, thermal and viscous effects are present throughout the film.

7. THE VELOCITY FIELD AND FILM THICKNESS

In view of [4] the pressure across the film layer is taken as constant. The remaining equations for velocity and temperature are uncoupled. Consequently, an attempt is made initially to evaluate the flow field and the film thickness. Approximate solutions have been obtained using Kármán–Pohlhausen momentum integral techniques.

Region I

Under appropriate boundary conditions the equation for the boundary layer thickness δ_1 is

$$\frac{\mathrm{d}}{\mathrm{d}x}\delta_1^2 = \frac{-7.160}{\epsilon}\sin x\delta_1^2 + 10.039\frac{\beta}{\mathrm{Fr}}. \qquad [10]$$

The numerical values arise from the use of an approximating velocity profile $u = U_0 f(\eta)$, where $f(\eta)$ is the similarity solution of Watson (1964) (see the appendix) based on $\eta = y/\delta(x)$, with $\delta(x)$ the length scale of viscous diffusion. The initial boundary layer thickness is of the order of the terms neglected in obtaining the reduced momentum and energy equations. Thus, using the approximate initial condition $\delta_1 = 0$, integration of [10] facilitates the estimation of x_0, the point at which viscous effects penetrate the surface, and $\delta(x_0)$ which may be used as initial data for the solution appropriate to Region II.

Region II

The equation which is valid when viscous effects are important throughout the film is

$$\frac{\mathrm{d}}{\mathrm{d}x}\int_0^{\delta(x)} u^2\,\mathrm{d}y = \frac{1}{\epsilon}\sin x\delta(x) - \frac{\beta}{\mathrm{Fr}}\left(\frac{\partial u}{\partial y}\right)_{y=0}, \qquad [11]$$

where the kinematic condition $v = u\,\partial\delta/\partial x$ has been invoked at the free surface. Following Smith (1971) a solution of the form $u = U(x)F(\eta)$ is postulated, where $U(x)$ and η are as specified earlier

and where $F(\eta)$ is an assumed quartic profile whose coefficients satisfy the boundary conditions

$$\frac{\partial^2 u}{\partial y^2} = -\frac{\sin x}{\mathrm{Fr}} \qquad \text{on} \quad y = 0,$$

$$u = U(x), \quad \frac{\partial u}{\partial y} = 0, \quad \frac{\partial^2 u}{\partial y^2} = -U\frac{\mathrm{d}U}{\mathrm{d}x} - \frac{\sin x}{\mathrm{Fr}} \quad \text{on} \quad y = \delta(x). \qquad [12]$$

Solutions based upon the respective equations have been obtained for various Re_{h_0} for fixed ratios h_0/a_0 using estimates of the stagnation layer thickness at $x = 0$. In figure 7 predicted film thicknesses are compared with the equivalent Nusselt forecast.

The differences are most marked in the vicinity of the top of the cylinder. Taking account of the initial momentum of the inundating flow has led to much reduced estimates of film thicknesses. At high Reynolds number the inertial forces outweigh viscous retardation and effectively sweep fluid around the cylinder into the region where gravitational acceleration is significant. The film thickness profile is thus relatively flat as compared to that forecast at lower Reynolds numbers. Here the effect of viscous retardation at the wall is rather more pronounced, giving rise to a greater growth rate of film thickness before gravity again accelerates the fluid around the cylinder.

8. TEMPERATURE DISTRIBUTION AND HEAT TRANSFER

The object is to determine the developing temperature field within the framework of a known velocity field. If the Prandtl number of the condensate is >1 the temperature effects will penetrate the free surface at a location further displaced around the cylinder than x_0. Accordingly, the temperature field is obtained by separate examination of three regions, as illustrated in figure 6, appropriately blended to provide a composite representation. Here, as suggested by Kutateladze *et al.* (1985), it is assumed that the temperature of the draining condensate is equal to the saturation temperature.

Region I

The thermal boundary layer thickness is denoted by δ_T and $\eta_\mathrm{T} = y/\delta_\mathrm{T}$, then $\eta = \lambda\eta_\mathrm{T}$, where λ is the ratio $\delta_\mathrm{T}/\delta_1$. Assuming a linear temperature distribution across the thermal layer leads to the following equation for λ:

$$\frac{\mathrm{d}}{\mathrm{d}x}[H_1(\lambda)\delta_1] = \frac{\beta}{\mathrm{Fr}\lambda\beta_1}, \qquad [13]$$

where $H_1(\lambda) = \lambda^2/3 - \lambda^4/10 + \lambda^5/30$. Simultaneous solution with the equation for the boundary layer thickness δ_1 establishes the temperature distribution in Region I.

Region II

In this region the constraint of conservation of volumetric flow rate simplifies the integrated energy equation to

$$\frac{\mathrm{d}}{\mathrm{d}x}\int_0^{\delta_\mathrm{T}} u\theta \,\mathrm{d}y = -\frac{\beta}{\mathrm{FrPr}}\left(\frac{\partial\theta}{\partial y}\right)_{y=0}. \qquad [14]$$

Using the velocity profiles of Region II once again leads to an equation for λ which may be solved simultaneously with that for δ in this region.

Region III

Prescribed profiles of temperature and velocity in terms of $\eta = y/\delta(x)$ lead to a straighforward equation of exponential decay with coefficients dependent on the profiles chosen and coupled to the film thickness δ. The solutions resulting from Regions I–III provide estimates of the temperature gradient at the cylinder surface around the cylinder from which heat transfer coefficients may be evaluated. Favourable comparison between the heat transfer coefficients obtained and recent experiments of Aidoun (1984) are illustrated in figure 3. These are presented for a range of flow rates, whose modes of drainage may be represented by the present theory. Also included are the equivalent Nusselt results.

9. DISCUSSION

Photographic observation of condensate film thickness at the point of re-attachment has shown that for both column and partial film drainage the film appears to behave more like a deflected jet than as a film of gradually reducing thickness as predicted by Nusselt. An accurate description for this region, where the condensate film is thinnest, is important, because here the heat transfer coefficient is highest. A stagnation theory allowing for the transformation of the radially flowing jet into an angularly flowing film has been outlined to describe the behaviour at the point of re-attachment. In contrast with previous workers, e.g. Kutateladze *et al.* (1985) and Jacobs & Nadig (1984), the analysis of the developing film thickness provides the background for the estimates of heat transfer characteristics as opposed to the Nusselt film thickness profile.

The difference in film thickness is shown in figure 7 where the dimensional film thickness variation around the tube is compared with the Nusselt result for $Re_{h_0} = 500$ and 1000. The difference in shape is most marked over the first 25–30° with the two-dimensional jet spreading out and flowing around the cylinder with thicknesses of the same order as the jet thickness. The Nusselt theory, on the other hand, predicts infinite film thicknesses at the top of the tube which reduce as the film velocity increases with angle ϕ. Over the remainder of the tube, the predicted film thickness is considerably less than the Nusselt value.

The theoretical heat transfer coefficient is shown in figure 3 and is seen to approach the experimental results at a Reynolds number of about 1000, i.e. at about the start of fully developed film drainage. The Nusselt prediction, which is known to be conservative, is shown for comparison. In the calculation of the heat transfer coefficients it should be noted that no provision for added mass of condensate due to condensation has been made as this mass was assumed to be small compared to the drainage flow. Justification for this procedure can be drawn from the experimental results in figure 3 where the results for the three tubes are almost coincident at the higher Reynolds numbers, showing that the additional condensate makes little difference to the heat transfer coefficient.

10. CONCLUDING REMARKS

Heat transfer coefficients for steam condensing under the influence of inundation have been determined for a wide range of experimental conditions. An alternative model to that of Nusselt for the asymptotic state of film drainage has been presented. Estimates of heat transfer coefficients from the theory compare favourably with the experimental results, even for the column mode of drainage, but the comparison improves as film drainage Reynolds numbers are approached.

REFERENCES

AIDOUN, Z. L. 1984 The effect of drainage on condensation heat transfer. Ph.D. Thesis, Univ. of Strathclyde, Glasgow.

BERMAN, L. D. & TUMANOV, Y. A. 1962 Investigation of heat transfer during the condensation of flowing steam on a horizontal tube bundle. *Teploenergetika* **9,** 77–88.

BUTTERWORTH, D. 1981 Inundation without vapour shear. In *Power Condenser Heat Transfer Technology* (Edited by MARTO, P. J. & NUNN, R. H.), pp. 271–277. Hemisphere/McGraw-Hill, Washington, D.C./New York.

FUJII T. & ODA, K. 1983 Condensation in tube banks. *J. chem. Engng Symp. Ser.* **75,** 3–22.

FUKS, S. N. 1957 Heat transfer with condensation of steam flowing in a horizontal tube bundle. *Teploenergetika* **4,** 35–38. NEL Translation No. 1041.

GRANT I. D. R. & OSMENT, B. D. J. 1958 The effect of condensate drainage on condenser performance. NEL Report No. 350.

JACOBS, H. R. & NADIG, R. 1984 Condensation on a film flowing over single and multiple isothermal horizontal tubes. *Proc. ASME* **38,** 115–121.

KERN, D. Q. 1958 Mathematical development of loading in horizontal condensers. *J. Am. Instn chem. Engrs* **4**(2), 157–160.

KUTATELADZE, S. S., GOGONIN, I. I. & SOSANOV, V. I. 1985 The influence of condensate flow rate on heat transfer in film condensation of stationary vapour on horizontal tube banks. *Int. J. Heat Mass Transfer* **28**(5), 1011–1018.

MAYHEW Y. R. 1981 Additional observations on vapour shear and condensate inundation. In *Power Condenser Heat Transfer Technology* (Edited by MARTO, P. J. & NUNN, R. H.), pp. 229–257. Hemisphere/McGraw-Hill, Washington, D.C./New York.

NICOL, A. A. & AIDOUN, Z. L. 1984 Simulated condensate film thickness and drainage studies. *Proc. 1st U.K. natn Heat Transfer Conf.* **1**, 649–658.

NOBBS, S. W. & MAYHEW, Y. R. 1975 Effect of downward vapour velocity and inundation on condensation rates on horizontal tube banks. *Steam Turbine Condensers*, NEL Report No. 619, pp. 39–52.

NUSSELT, W. 1916 The surface condensation of water vapour. *Z. Ver. dt. Ing.* **60**, 541–546, 569–575. Translated in *Chem. Engng Fundam.* **1**(2), 6–19 (1982).

SHKLOVER, G. G. & BUEVICH, A. V. 1978 The mechanism of film flow with steam condensation in horizontal bundles of tubes. *Teploenergetika* **25**(4), 62–65.

SHORT, B. E. & BROWN, H. E. 1951 Condensation of vapours on vertical banks of horizontal tubes. *Proc. Inst. mech. Engrs General Discussion on Heat Transfer*, pp. 27–31.

SMITH, S. H. 1971 Boundary layer flow in a thin sheet of viscous liquid. *J. Engng Math.* **5**, 11–18.

WATSON, E. J. 1964 The radial spread of a liquid jet over a horizontal plane. *J. Fluid Mech.* **20**, 481–499.

APPENDIX

The Watson similarity profile $f(\eta)$ is the solution of the differential equation

$$\frac{\mathrm{d}^2 f}{\mathrm{d}\eta^2} + \frac{3}{2} c^2 f^2 = 0,$$

subject to the boundary conditions

$$f(0) = 0, \quad f(1) = 1, \quad f'(1) = 0.$$

The unique solution satisfying all the boundary conditions gives

$$c = \frac{\Gamma(\frac{1}{2})\Gamma(\frac{1}{3})}{3\Gamma(\frac{5}{6})} .$$

A useful integral property of $f(\eta)$, required when implementing the profile in a Kármán–Pohlhausen method, can be obtained analytically as

$$\int_0^1 f(\eta)\,\mathrm{d}\eta = \frac{2\pi}{3\sqrt{3}c^2} .$$